In-depth characterisation of metal-support compounds in spent Co/SiO_2 Fischer-Tropsch model catalysts

Moritz Wolf[a,1], Emma K. Gibson[b,c], Ezra J. Olivier[d], Jan H. Neethling[d], C. Richard A. Catlow[b,e], Nico Fischer[a], Michael Claeys[a,]

[a] Catalysis Institute and DST-NRF Centre of Excellence in Catalysis c*change, Department of Chemical Engineering, University of Cape Town, Private Bag X3, Rondebosch, 7701, South Africa
[b] UK Catalysis Hub, Research Complex at Harwell, RAL, Oxford, OX11 0FA, United Kingdom
[c] School of Chemistry, University of Glasgow, Glasgow, G12 8QQ, United Kingdom
[d] Centre for High Resolution Transmission Electron Microscopy, Physics Department, Nelson Mandela University, PO Box 77000, Port Elizabeth, 6031, South Africa
[e] Department of Chemistry, University College London, London, WC1H 0AJ, United Kingdom

ARTICLE INFO

Keywords:
Cobalt catalyst
Metal-support compound
Cobalt silicate
XANES
TEM

ABSTRACT

Only little is known about the formation and morphology of metal-support compounds (MSCs) in heterogeneous catalysis. This fact can be mostly ascribed to the challenges in directly identifying these phases. In the present study, a series of Co/SiO_2 model catalysts with different crystallite sizes was thoroughly characterised with focus on the identification of cobalt silicate, which is the expected metal-support compound for this particular catalyst system. The catalysts were exposed to simulated high conversion Fischer-Tropsch environment, i.e. water-rich conditions in the presence of hydrogen. The transformation of significant amounts of metallic cobalt to a hard-to-reduce phase has been observed. This particular MSC, Co_2SiO_4, was herein identified as needle- or platelet-type cobalt silicate structures by means of X-ray spectroscopy (XAS) and high-resolution scanning transmission electron microscopy (HRSTEM) in combination with elemental mapping. The metal-support compounds formed on top of fully SiO_2-encapsulated nanoparticles, which are hypothesised to represent a prerequisite for the formation of cobalt silicate needles. Both, the encapsulation of cobalt nanoparticles by SiO_2 via creeping, as well as the formation of these structures, were seemingly induced by high concentrations of water.

1. Introduction

Strong metal-support interaction (SMSI) in heterogeneous catalysts refers to catalytically active metal particles that are strongly bound to the support via chemical solid-state reactions between metal atoms and the support [1]. Such a formation of metal-support compounds (MSC) consequentially results in deactivation due to inferior chemisorption and catalytic properties. Self-diffusion, diffusion through the interface, and diffusion into the second solid phase represent the three stages preceding the chemical solid-state reactions of two solid phases being in close proximity. Depending on the diffusion coefficients of the parti-cular atoms, the reaction either occurs on one side or on both sides of the transition region. Unless one of the reacting phases is present as small nanoparticle and hence may be transformed as a whole, the transition region is typically saturated by the formed compound hin-dering continuous diffusion of atoms to the reaction front and hence isolating the two solid phases [2].

The experimental characterisation of MSCs is challenging as pre-sumably thin layers are formed at the interface between metallic par-ticles and the support due to the diffusion limited reaction of atoms of the solids [2]. For example, the layer thickness may be below the lower detection limit of X-ray diffraction (XRD) analysis. Standard char-acterisation techniques such as temperature programmed reduction (TPR) showing the reduction of MSCs at increased temperatures [3–11] or thermogravimetric analysis (TGA) [6,8,12,13] have been applied for the identification of MSCs in the literature, but these do not char-acterise the phase of interest directly. In contrast, X-ray absorption spectroscopy (XAS) is ideally suited to identify MSCs in catalysts due to its high sensitivity towards different oxidation states, coordination number, as well as neighbouring atoms and it has been widely applied for the identification of cobalt aluminates in various Co/Al_2O_3 catalysts after application in the Fischer-Tropsch (FT) synthesis [11,13–18]. The

Corresponding author.
E-mail address: michael.claeys@uct.ac.za (M. Claeys).
[1] Present address: Institute of Chemical Reaction Engineering, University of Erlangen-Nuremberg, 91058 Erlangen, Germany.

use of microscopy-based techniques for the direct identification of MSCs has been scarcely reported in literature. To our knowledge, only Kiss et al. successfully identified cobalt silicate-type structures in a spent $Co/Re/SiO_2$ FT catalyst in 2003 [19].

The main product of the FT synthesis is H_2O, which has been linked to deactivation of cobalt-based FT catalysts [10,18,20–26]. Three me-chanisms have been proposed in literature: hydrothermal sintering of cobalt particles leading to a loss of specific surface area [23,27], oxi-dation of metallic cobalt to FT inactive cobalt oxides [24–26], and the formation of MSCs [18,19], which are also not active for the FT synthesis [20]. In the aforementioned study by Kiss et al., a partially reversible deactivation of the $Co/Re/SiO_2$ catalyst has been reported after high conversion (90–100%) FT synthesis in a fixed-bed reactor (FBR) at 20 bar and 220 °C (H_2:CO = 2.1) [19]. No such deactivation behaviour was observed for lower CO conversion levels of 50–55%. Hence, the presence of a large concentration of H_2O at increased con-version levels may have induced the formation of MSCs, which has been shown in situ for Al_2O_3-supported FT catalyst by Tsakoumis et al. in a more recent study [18]. For the first time, Kiss et al. observed clay-like structures in the spent $Co/Re/SiO_2$ catalyst after high conversion FT synthesis by means of transmission electron microscopy (TEM), which were identified as cobalt silicate-type species via energy-dispersive spectroscopy (EDS). These needle- or platelet-like structures were also identified in a reduced and steam-treated catalyst demonstrating the exacerbating effect of H_2O on the stability of the Co phase. However, no MSC compound could be detected by means of XRD analysis [19]. In-terestingly, the identified MSC was partially reducible at 420 °C and further strongly resembles phyllo-silicates, which have been synthe-sised as a precursor in various catalyst preparation routes [28–32].

In the present study, a series of spent Co/SiO_2 model FT catalysts has been thoroughly characterised with focus on direct identification of potentially formed cobalt silicates. It has to be noted, that the low Co loading of 0.4 wt.% precludes indirect characterisation methods such as TGA or TPR analyses. The samples were applied in a previous study [33], which reported the formation of hard-to-reduce species during exposure to simulated high conversion FT environment using an in situ magnetometer. Oxidation of Co was observed and could only be par-tially reversed in a re-reduction experiment, which strongly suggests the formation of hard-to-reduce cobalt silicate [34]. A size-dependent oxidation behaviour was identified as more metallic Co was trans-formed into oxidic species for smaller crystallite sizes. Additional ex-periments including the second FT reactant CO in the feed indicated an enhancement of H_2O-induced oxidation of Co to CoO [33], which was recently unveiled in a separate study [24]. Herein, the five spent and passivated samples were now characterised in depth by means of TEM and XAS in order to confirm the formation of cobalt silicate species via direct characterisation of MSCs. Furthermore, these techniques may allow for a quantification and provide insight into the morphology and formation of the identified hard-to-reduce phases.

2. Material and methods

2.1. Catalyst preparation

The herein characterised spent Co/SiO_2 catalysts were prepared and tested in our previous work (ref. [33]). Three different sizes of well-defined Co_3O_4 nanoparticles (3, 5, and 7 nm) were synthesised (Figure S1-S3; Table S1-S2) applying a sol-gel route in the absence of classical surfactants [33,35,36]. In short, cobalt acetate tetrahydrate was dis-solved in benzyl alcohol under magnetic stirring (500 rpm) in a round bottom flask for 2 h. A 25 wt.% aqueous ammonium hydroxide solution was added dropwise and the flask was transferred to a preheated oil bath (165 °C) in a rotary evaporator and heated for 3 h (0.9 bar, 180 rpm). Air was bubbled through the solution to provide adequate mixing of the emulsion [36]. After cool down to room temperature, the volume was tripled with diethyl ether and the mixture was centrifuged for 1 h at 7000 rpm. Lastly, the centrifugate was purified in several cycles of re-dispersion in ethanol and centrifugation in an excess of acetone.

Stöber silica spheres [37] were prepared at room temperature under continuous magnetic stirring at 1000 rpm [33,38]. In short, 300 mL iso-propanol and 22.5 mL H_2O were mixed in an Erlenmeyer flask. A total of 3.63 g of a 25 wt.% aqueous ammonium hydroxide solution was added after 10 min and the mixture was stirred for another 10 min. Stöber spheres were formed during the addition of 41.88 mg of tetra-ethyl orthosilicate over 1 min and an ageing of 5 h. Lastly, the Stöber spheres were collected via centrifugation, washed several times with 70% ethanol in H_2O, and dried in an oven at 120 °C for 24 h.

For the preparation of the model catalysts, the separately synthe-sised Co_3O_4 crystallites were dispersed in ethanol in an ultrasonic bath until all particles were in dispersion. Stöber silica spheres were soni-cated for 4 h in ethanol in a separate beaker. Afterwards, the dispersion of Co_3O_4 crystallites in ethanol was added dropwise targeting a loading of 0.5 wt.% metallic cobalt. After sonicating for another 4 h, the dis-persion was transferred to a rotary evaporator and mixed at 80 °C for 1 h (1 bar, 240 rpm). Subsequently, ethanol was evaporated from the parent catalyst at 0.462 bar resulting in well-dispersed Co_3O_4 crystal-lites over the surface area of SiO_2 Stöber spheres (Figure S3) as pre-viously reported [33].

2.2. Exposure to H_2O-rich environment

The stability of the prepared model catalysts was tested under H_2O-rich environment in an in situ magnetometer [39], which is highly sensitive towards the presence of ferromagnetic metallic Co. However, it cannot identify nor distinguish between the various oxidic cobaltous species at temperatures exceeding room temperature. Details on the experimental set-up and methodology of the magnetometer can be found elsewhere, e.g. ref. [21,23,24,33,39]. In our previous work [33], a total amount of 2003.6 mg of the particular catalyst was loaded and reduced in 50% H_2/Ar at moderate temperatures (300–400 °C and 1 °C min^{-1}; Figure S4) successfully preventing sintering (Table 1; Figure S5). Subsequently, the catalysts were exposed to p_{H2}/p_{H2O} ratios (FT reaction over FT product) of 0.15–50 mimicking FT conversion levels in the range of 26–99% (Table 2; Figure S4; Table S3). Some of the samples were exposed to reducing conditions (15% H_2/Ar) up to the maximum reduction temperature to test for reducible fractions (Table 2; Figure S4). Lastly, the samples were passivated in 1% O_2/N_2 [40] to prevent uncontrolled oxidation of metallic Co upon exposure of the samples to atmospheric air during transport to post-run character-isation facilities (Figure S6).

2.2.1. Transmission electron microscopy (TEM)

The spent catalysts were mixed with acetone and dispersed via ul-trasonication for 3 min. The dispersion was subsequently deposited onto carbon-coated copper grids for analysis via TEM. Samples were analysed in a Tecnai F20 microscope (Philips) equipped with a field emission gun and operated at 200 kV. The TEM has a built-in US4000 4kX4k CCD camera (Gatan). High-resolution scanning transmission electron microscopy (HRSTEM) images were acquired at atomic

Table 1
Volume mean crystallite size of metallic cobalt in the characterised model catalysts after reduction in H_2 as obtained by analysis of the magnetisation as a function of the external field strength. Data is reproduced from ref. [33] with permission from The Royal Society of Chemistry.

Sample	Co loading / wt.%	Crystallite size of Co^0 / nm
CAT A	0.42	3.2
CAT B	0.43	5.3
CAT C	0.41	6.7

Table 2

Experimental details of the exposure of the model catalysts following reduction in H_2.

Sample	p_{H2}/p_{H2O}	p_{H2}/p_{CO}	Re-reduction	Passivation
CAT A1, CAT C	0.15, 1.5, 5, 10, 20, 30, 40, 50, ∞, 0	∞	Yes	Yes
CAT A2	40	∞	Yes	Yes
	40, 0	2.1		
	0	∞		
CAT B1	0.15, 1.5, 5, 10, 20, 30, 40, 50	∞	No	Yes
CAT B2	0, 0.15, 1.5, 5, 10, 20, 30, 40, 50, 0	2.1	Yes	Yes
	0	∞		

resolution using a double spherical aberration corrected JEM-ARM200 F microscope (JEOL). The instrument has an advanced GIF electron spectrometer with dual electron energy loss spectrometry (EELS) imaging capabilities, as well as an XMax 100 TLE high collection angle, ultra-sensitive detector (Oxford Instruments) for analysis by means of energy-dispersive spectrometry (EDS). A fast Fourier trans-form (FFT) analysis was conducted on selected areas of high resolution micrographs for the measurement of inter-planar spacings. Quantifoil sample grids were utilised for HRSTEM purposes.

2.2.2. X-ray absorption spectroscopy (XAS)

XAS spectra were acquired at beamline B18 of the Diamond Light Source in Harwell (United Kingdom) [41]. Additional standards were prepared via published synthesis routes (CoO (fcc): ref. [36]; γ-Co_2SiO_4 (normal spinel): ref. [42]) and characterised by means of XRD and TPR (Figure S11−S12), while the as prepared nanoparticles for CAT C were applied as standard for Co_3O_4. All standards were analysed in trans-mission mode with three repetitions, while the actual samples were measured in fluorescence mode with 12 repetitions. All spectra were acquired at the Co K-edge and with a Co foil (Sigma-Aldrich) placed before the reference detector. The raw data was processed in Athena, a tool of the open-source software package Demeter [43], which is based on the IFEFFIT library [44]. Linear combination fitting (LCF) of the X-ray absorption near edge structure (XANES) spectra of the spent and passivated samples with the particular standards was conducted in the first derivative of the normalised absorption in the energy range of −20 to 50 eV relative to the sample's edge utilising Athena. Reported R-factors represent the mean square sum of the misfit for all data points within the fitting region.

3. Results and discussion

The five spent and passivated Co/SiO_2 model catalysts were ana-lysed by means of XAS in order to identify the coordination of Co atoms. The samples can be expected to feature SiO_2 as the support material of choice and three cobaltous phases. Firstly, metallic Co is present, which was detected and monitored during passivation of the samples in 1% O_2/Ar [40] in the magnetometer (Figure S6) [33]. Secondly, the ap-plied treatment has been reported to exclusively form CoO, i.e. the controlled oxidation of Co nanoparticles does not result in the forma-tion of Co_3O_4 [40]. Lastly, the formation of a hard-to-reduce species was identified as a re-reduction at moderate temperatures did not re-cover previously oxidised Co [33]. Indeed, comparison of a XANES spectrum obtained for the as prepared Co_3O_4 nanoparticles, which have been applied in the preparation of CAT C as well, with the spectra of the spent catalysts clearly demonstrates the absence of Co_3O_4 (Figure S7). Said phase features a distinct edge shift to higher energies and pro-nounced white line characteristics, which cannot be identified in any of the spent catalysts. Hence, only the spectra of metallic Co, CoO, and a cobalt silicate were applied as standards.

The intensity of the normalised absorption of the shoulder

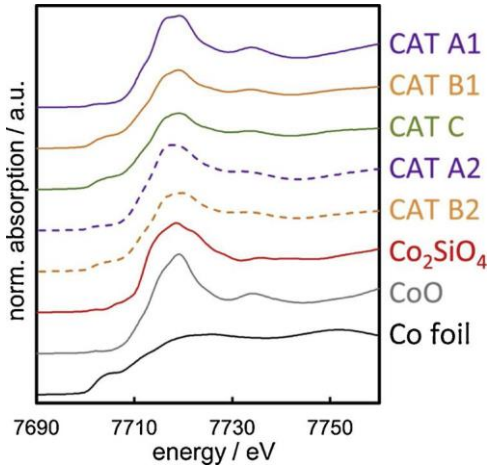

Fig. 1. Normalised X-ray absorption near edge structure spectra of the spent and passivated model catalysts after exposure to water-rich environment with spectra of standards.

(7702 eV) of the main edge (7709 eV) to lower energy levels directly correlates to the amount of metallic Co in each sample as, out of all measured standards, only Co foil displays a pronounced pre-edge structure [45] (Fig. 1). In situ magnetic measurements during the ex-posure to H_2O-rich environment exhibited a pronounced oxidation of the smaller nanoparticles in CAT A [33]. In accordance with these observations, the samples containing larger nanoparticles (CAT B1, CAT B2, CAT C) show distinct shoulders of the main edge due to the pro-nounced pre-edge features of metallic Co (Table 3). The presence of metallic Co is further suggested by smaller edge shifts of the spent samples when compared to the CoO and Co_2SiO_4 standards. This shift typically shows a linear dependency on the valency of the metal and increases with oxidation state [46–48]. Hence, the average oxidation state of Co in all five samples can be expected to be between 0 and 2. Further, the intensities of the white lines decrease with increasing in-itial size of Co nanoparticles, i.e. Co atoms in the samples containing smaller nanoparticles have a higher average degree of oxidation.

Linear combination fitting (LCF) of the XANES spectra with the standards allows for a quantitative analysis of the cobaltous phases present in the spent catalysts. Fitting the spectra in the first derivative with references (Co foil, CoO, Co_2SiO_4) provides reasonable fits for all five samples, i.e. all features of the spectra are covered by the standards suggesting the absence of additional phases (Fig. 2). It has to be noted that including Co_3O_4 as a standard resulted in 0% of Co atoms being associated to this phase for any sample and any combination of stan-dards demonstrating the absence of this phase in the spent catalysts. As indicated by the normalised pre-edge intensities (Table 3), only small amounts of metallic Co are present in both spent catalysts CAT A1 and CAT A2 comprising the smallest nanoparticles (Table 4). In fact, all Co atoms in CAT A1 are seemingly associated with either CoO or cobalt silicate, which would then explain the absence of any oxidation during

Table 3

Characteristics of the X-ray absorption near edge structure spectra of selected standards and spent and passivated model catalysts.

Sample	Normalised pre-edge intensity	Edge shift / eV	Normalised white line intensity
CoO	0.04	4.6	1.62
Co_2SiO_4	0.06	4.8	1.49
CAT A1	0.07	1.5	1.43
CAT A2	0.08	1.9	1.39
CAT B1	0.22	1.4	1.28
CAT B2	0.17	2.0	1.29
CAT C	0.21	1.3	1.25

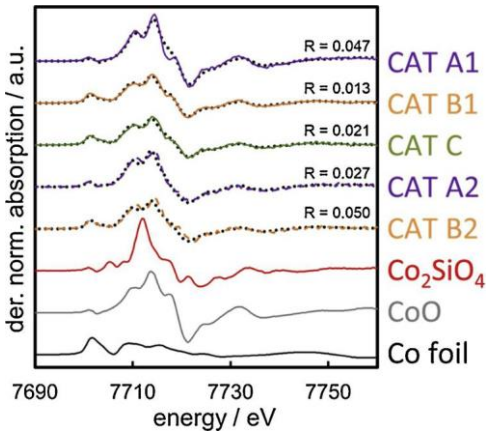

Fig. 2. First derivatives of normalised X-ray absorption near edge structure spectra of the spent and passivated model catalysts and standards (solid), as well as the linear combination fits with the standards in the range of −20 to 50 eV relative to the edge (dotted) with R-factors.

Table 4
Degree of reduction to metallic cobalt of the model catalysts according to magnetic measurement after passivation and phase compositions with parti-cular errors according to the linear combination fits of X-ray absorption near edge structure spectra with the particular standards.

Sample	DOR / %	Co / %	CoO / %	Co_2SiO_4 / %
CAT A1	14	0	56.6 ± 3.3	43.4 ± 3.3
CAT A2	13	17.5 ± 1.2	24.1 ± 2.1	58.4 ± 2.4
CAT B1	53	43.1 ± 0.7	39.1 ± 1.2	17.8 ± 1.4
CAT B2	44	41.7 ± 1.3	29.0 ± 2.4	29.3 ± 2.8
CAT C	52	45.8 ± 0.8	31.4 ± 1.5	22.7 ± 1.7

passivation of this catalyst (Figure S6). However, the catalyst displayed a limited susceptibility to magnetisation upon passivation corre-sponding to a degree of reduction (DOR) to metallic Co of 14% (cor-responding to an absolute amount of 1.2 mg). It has to be noted that the high sensitivity of the magnetometer towards ferromagnetic phases allows for an accurate quantification of 1 mg of Co and the qualitative detection of even smaller amounts of metallic Co (0.1 mg or even less). In addition, the applied passivation technique has been reported to protect a metallic core for an extended time range [40]. Hence, quan-tification via LCF of XANES spectra potentially lacks in accuracy. Either way, the distinct identification of Co_2SiO_4 results in 50% of the Co atoms being present as cobalt silicate, which is the phase of interest for the conducted analyses (the phase concentrations of Co and CoO were altered by the re-reduction and passivation). The same catalyst was also exposed to a p_{H2O}/p_{H2} ratio of 40 in the absence of CO and subsequent exposure to a low partial pressure of synthesis gas (CAT A2) [33]. This sample oxidised to a small extent during passivation and, indeed, LCF of the XANES spectra suggests the presence of metallic Co.

LCF of catalysts with larger nanoparticles results in 42–46% of Co atoms found in the metallic state, which corresponds fairly well with the residual DOR after passivation (Table 4). It has to be noted that the initial DOR to metallic Co before exposure to water-hydrogen mixtures was 56% for CAT B and 83% for CAT C. Hence, significant amounts of CoO were still present in these catalysts after reduction in H_2 [33]. While our previous study focused on the H_2O-induced formation of MSCs from the metallic Co phase, most published studies on deactiva-tion of FT catalysts assume an exclusive formation of MSCs via CoO [11,18,49–51]. Indeed, the relatively high fraction of a $Co_xSi_yO_z$ phase close to the stoichiometric composition of the Co_2SiO_4 standard in the present study exceeds the expected formation of MSCs from the metallic Co phase (< 10% according to in situ magnetic measurements [33]), which strongly suggests the additional formation of MSCs from CoO nanoparticles. This explanation is in accordance with thermodynamic predictions for bulk phase solid-state reactions as CoO is in particular

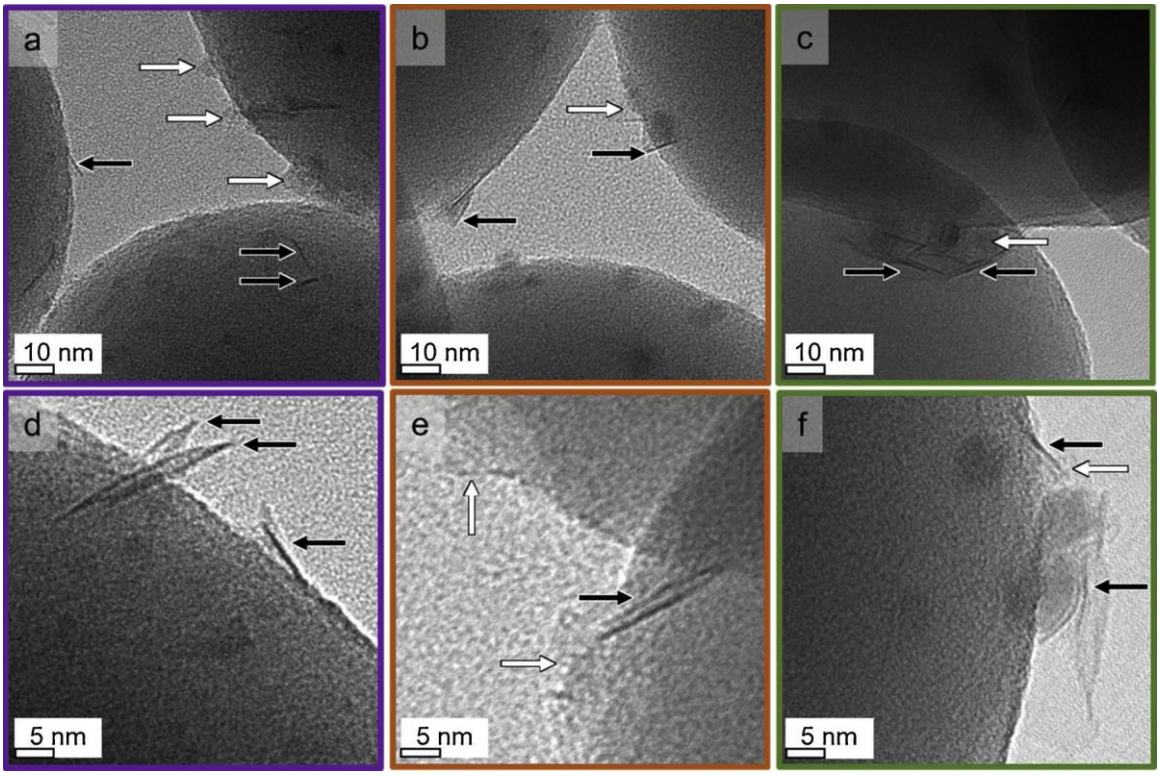

Fig. 3. Transmission electron micrographs of spent and passivated model catalysts (a) CAT A1, (b) CAT B1, as well as (c) CAT C and (d–e) enlarged images of needle-like structures (demarked with black arrows) on top of nanoparticles surrounded by a cloud of material with different density (demarked with white arrows).

prone to form MSCs with SiO_2 [52], especially when compared to the H_2O-induced formation of $Co_xSi_yO_z$ from the metallic Co phase [33].

After direct identification of cobalt silicates in the spent catalysts, the morphology of the nanoparticles in CAT A1, CAT B1, and CAT C was analysed via conventional TEM. Almost all nanoparticles in the spent samples feature a second, rather bulky phase surrounding presumably metallic cores (Fig. 3). The thickness of this second phase exceeds the expected dimensions of a CoO shell from passivation in 1% O_2/Ar (approximately 1–1.5 nm) [40]. Larger nanoparticles are surrounded by a cloud of material which appears to have a significantly lower density than that of the cobalt particles. The smaller nanoparticles in catalyst CAT A1 and, less pronounced, in CAT B1 are mostly accompanied by a needle-type structure suggesting the presence of phyllosilicate (Fig. 3; Figure S8). Only a small fraction of the larger nanoparticles in CAT C features such needles, which corresponds to the identified less pro-nounced formation of $Co_xSi_yO_z$ in this catalyst. These clay-type struc-tures have been reported by Kiss et al. for rhenium-promoted and fumed SiO_2-supported Co catalysts after high FT conversion testing, as well as after hydrothermal treatment [19]. In said study, the needles were identified as cobalt-silica mixed oxide phase via energy-dispersive spectroscopy (EDS) in TEM.

Analysis of the morphology of the cloudy phase surrounding Co nanoparticles and the needle-type structures in the spent catalyst CAT B1 was conducted via HRSTEM. Coupling HRSTEM with elemental mapping via EELS spectrum imaging allows for the direct identification of MSCs. In order to avoid background contributions from the SiO_2 support, only nanoparticles on the edge of the Stöber spheres were mapped revealing a full encapsulation of a metallic Co nanoparticle by SiO_2 (Fig. 4; Figure S9). Therefore, it can be concluded that the amorphous SiO_2 support must have become mobile during the exposure to H_2O-rich atmospheres, resulting in creeping of Si species onto the Co nanoparticles (Fig. 5). Such a complete encapsulation of the metallic phase may protect the core from oxidation during passivation, which

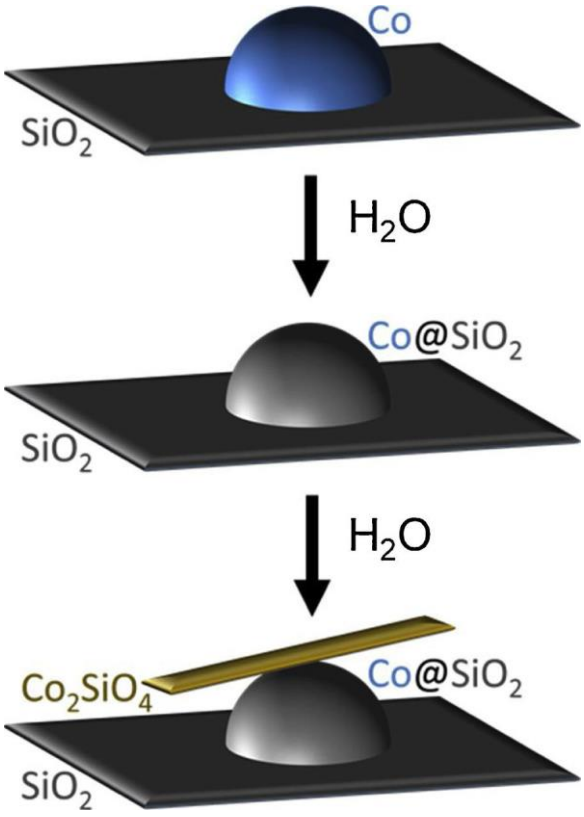

Fig. 5. Schematic of the proposed mechanism of silica encapsulation of cobalt nanoparticles and subsequent formation of needle-type cobalt silicate structures under water-rich conditions during Fischer-Tropsch synthesis.

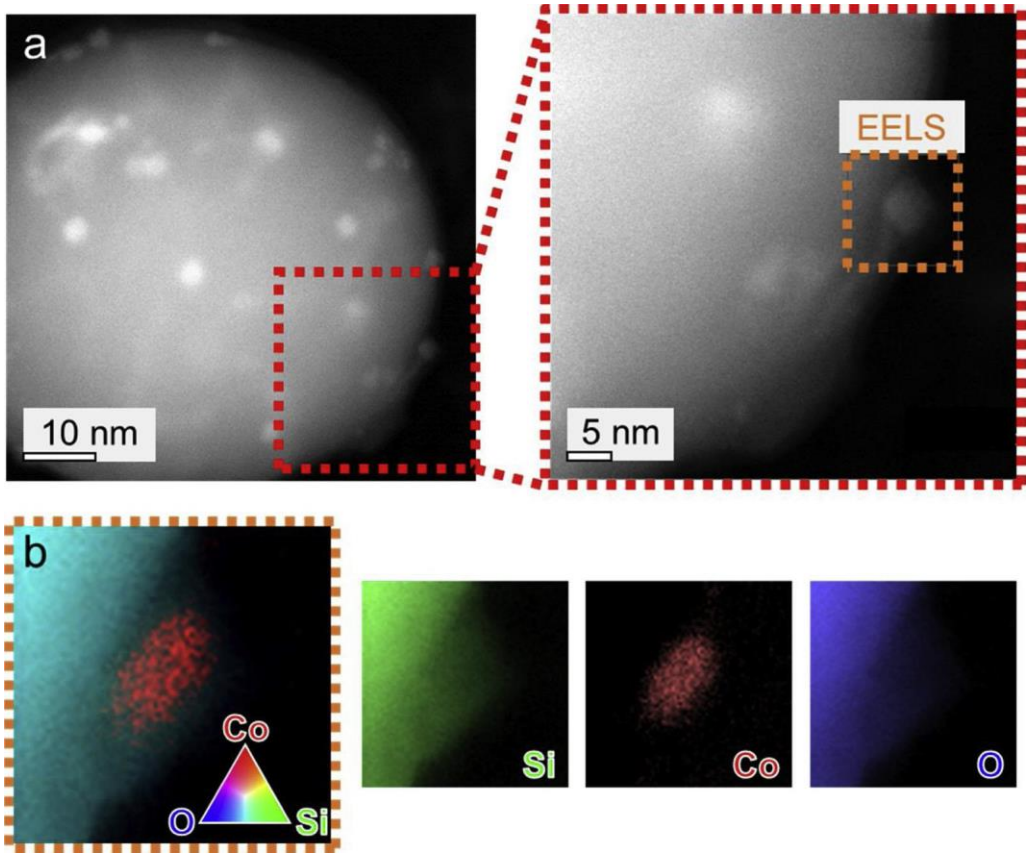

Fig. 4. (a) High-resolution high angle annular dark field transmission electron micrograph with a magnified area ex-hibiting a silica-encapsulated cobalt nanoparticle in the spent and passi-vated model catalyst CAT B1 and (b) elemental mapping of the inset as ob-tained via electron energy loss spectro-scopy with separate maps for the par-ticular elements.

represents a reasonable explanation for the absence of oxidation in the smallest Co nanoparticles (CAT A1), after prolonged exposure to H_2O-rich conditions (Figure S6). Creeping of SiO_2 in a Co/SiO_2 model cat-alyst has earlier been reported by Saib et al. [53], who referred to a mobile SiO_2 phase fully encapsulating and protecting 4 nm Co nano-particles on Stöber spheres from oxidation during hydrothermal treat-ment. However, this migration of SiO_2 was hypothesised to be induced by the harsh conditions required for reduction of the model catalyst at 500 °C in H_2. An experimental proof for this hypothesised encapsulation was only observed by means of HRTEM when reducing at even further increased temperatures of 700 °C in H_2. In contrast, the moderate conditions during reduction of the nanoparticles in the present study (300–400 °C) can be expected to prevent such migration of Si species during reduction. Further, a less pronounced interaction of the nano-particles with the support prior to and during reduction can be expected in the present study as no calcination was conducted. Lastly, adsorption effects of H_2O-originated species on the metallic Co surface [23] were observed during in situ magnetic measurements [33], i.e. the surface of Co nanoparticles was accessible for the gas phase after reduction in all samples. Even a size-dependency was observed due to the increasing specific surface area with decreasing average particle size [33]. Hence, the herein observed encapsulation occurred during exposure to in-creased H_2O/H_2 ratios only.

The continuous exposure of these encapsulated metallic nano-particles in combination with increased p_{H2O}/p_{H2} ratios in our previous study [33] may have induced the subsequent formation of $Co_xSi_yO_z$ needles (Fig. 5). The formation of such a MSC was identified by means of XANES (Fig. 2). In addition, EELS mapping of nanoparticle featuring needle- or platelet-like structures suggests the presence of Co, Si, and O atoms (Fig. 6a). It has to be noted that the energy-rich beam heavily interfered with the identified needle-type structures having a destruc-tive effect with prolonged exposure times during elemental mapping and resulting in a seemingly inhomogeneous elemental distribution (Figure S10). Nevertheless, the elemental maps clearly point towards the formation of a mixed metal oxide. Analysis of identified inter-planar spacings (approximately 2.2, 2.3, and 2.6 Å; Fig. 6b) by means of an FFT analysis of lattice resolved micrographs points towards the for-mation of an orthorhombic Co_2SiO_4 as the lattice planes corresponds to α-Co_2SiO_4 in the olivine structure or β-Co_2SiO_4, a modified spinel (Table S4) [54]. A distinct differentiation is challenging due to several similar inter-planar distances in both polymorphs of Co_2SiO_4 and the limited quality of the micrographs as a result of short exposure times to prevent the rapid destruction by beam interference. Either way, a full encapsulation of Co nanoparticles by SiO_2 is potentially required prior to the formation of this needle-type Co_2SiO_4. The increased dispersion of Co atoms in CAT A results in a larger mass specific interface area between the Co phase and encapsulating SiO_2. However, this difference cannot solely explain the significantly pronounced oxidation to MSCs when compared to larger nanoparticles. Hence, the hypothesis of full encapsulation representing a prerequisite for the formation of needle-type Co_2SiO_4 may explain the strong size-dependent stability in Co/ SiO_2 model catalysts during exposure to H_2O-rich conditions [33].

The herein presented work is meaningful for the FT community as the detailed characterisation of the spent Co/SiO_2 model catalysts provides insight into the feasibility and mechanism of water-induced deactivation. In the past, particularly deactivation of Co-based FT cat-alysts via formation of MSCs has been unsatisfactorily dealt with in literature. For example, vague terms such as "highly dispersed cobalt phase over the support" are widely applied in literature due to an un-successful identification [13,18,45,55–57]. The formation of these phases is, at least for Al_2O_3-supported Co, widely assumed to ex-clusively proceed via CoO [6,11,18,49–51]. However, the exposure of CAT A1, CAT B1, and CAT C to H_2O-rich atmospheres in the absence of CO can be expected to induce only marginal oxidation of metallic Co to CoO [24] as the FT conversion was fully simulated (no CO in feed stream) [33]. Furthermore, the partial pressure of CO (0.07 bar) in the experiments of CAT A2 and CAT B2 under H_2O-rich environment was recently shown to result in a slow, kinetically hindered oxidation to CoO only [24]. Hence, the present study provides experimental proof for the direct oxidation of metallic Co to MSCs in the case of SiO_2-supported model catalysts. At first, high concentrations of H_2O induce creeping of mobile SiO_2 species of the amorphous Stöber spheres onto the metallic nanoparticles and, in case of full encapsulation, such an encapsulation may allow for the formation of MSCs. It has to be noted, that this observation is the result of a fundamental study in the absence of promoters and using model catalysts with low cobalt loadings. Fur-ther, the applied conditions do not represent commercial FT environ-ment and hence drawn conclusions may not be directly applicable for catalysts under industrial conditions.

The presented results on the formation of cobalt-support compounds also point towards the importance of the catalyst preparation technique on the final stability of cobalt nanoparticles. Less oxidation to cobalt-support compounds can be expected for calcined catalysts than for the herein prepared catalysts via physical deposition of nanoparticles onto the supports without any thermal treatment. This highly relevant his-tory of the catalysts can be further demonstrated when comparing the present study with similar work by Kiss et al. [19] and Saib et al. [53]. In the former study, a (partially) reversible formation of cobalt silicate species was observed, while the MSC in the present study was stable up to 400 °C in (diluted) H_2. A pronounced interaction between the SiO_2 Stöber spheres as support material and the (partially) encapsulated Co nanoparticles can be expected for the prepared and reduced model catalysts by Saib et al. due to a rather harsh preparation, e.g. calcination and high reduction temperatures.

Lastly, a significant structure sensitivity of the FT performance has been identified for catalysts with Co crystallite sizes below 10 nm [58–65]. The turnover frequency (TOF) was identified to decrease with size even though smaller crystallites exhibit a higher specific surface area. However, the concentration of exposed active sites for the FTS decreases with size resulting in a lower activity [65–67]. The present study exhibits a size-dependency for both, the encapsulation of Co na-noparticles by SiO_2 and the consequential formation of MSCs, which is in line with findings by Saib et al. [53]. Larger nanoparticles are see-mingly less prone to encapsulation, which is induced by high con-centrations of H_2O and has recently been hypothesised for an Al_2O_3-supported, Re-promoted 20 wt.% Co catalyst as well [18]. Hence, loss of active Co during FTS can be limited by the preparation of relatively large nanoparticles close to the optimum size for high TOFs of ap-proximately 10 nm [58,62]. Furthermore, several studies based on adequate in situ characterisation of well-defined catalysts suggest the general absence of oxidation of Co to CoO for crystallite sizes larger than 4.5 nm under commercially relevant conditions with p_{H2O}/p_{H2} ratios below 2.2 corresponding to 81.5% CO conversion during FTS [11,24,26,33,68,69]. Hence, catalysts with Co crystallites of 10 nm are not only expected to result in the highest specific activity, but also exhibit an increased stability during the FTS. Nevertheless, smaller crystallites are typically present in most catalysts due to relatively wide size distributions and research on the deactivation of this fraction re-mains meaningful for the commercial application of the FTS.

4. Summary and conclusions

Spent Co/SiO_2 model catalysts from a study on the size-dependent, direct oxidation of Co nanoparticles in H_2O-H_2 mixtures were thor-oughly characterised. Application of adequate characterisation techni-ques targeted the direct identification of formed MSCs, in this case cobalt silicate-type species. Such a Co_2SiO_4 phase was identified in all spent catalysts by means of XANES, while microscopy-based char-acterisation techniques supported the formation of a mixed metal oxide phase. Needle-type cobalt silicates resembling a clay- and phyllosili-cate-type structure were formed on SiO_2-encapsulated cobalt nano-particles. Smaller nanoparticles displayed a pronounced formation of

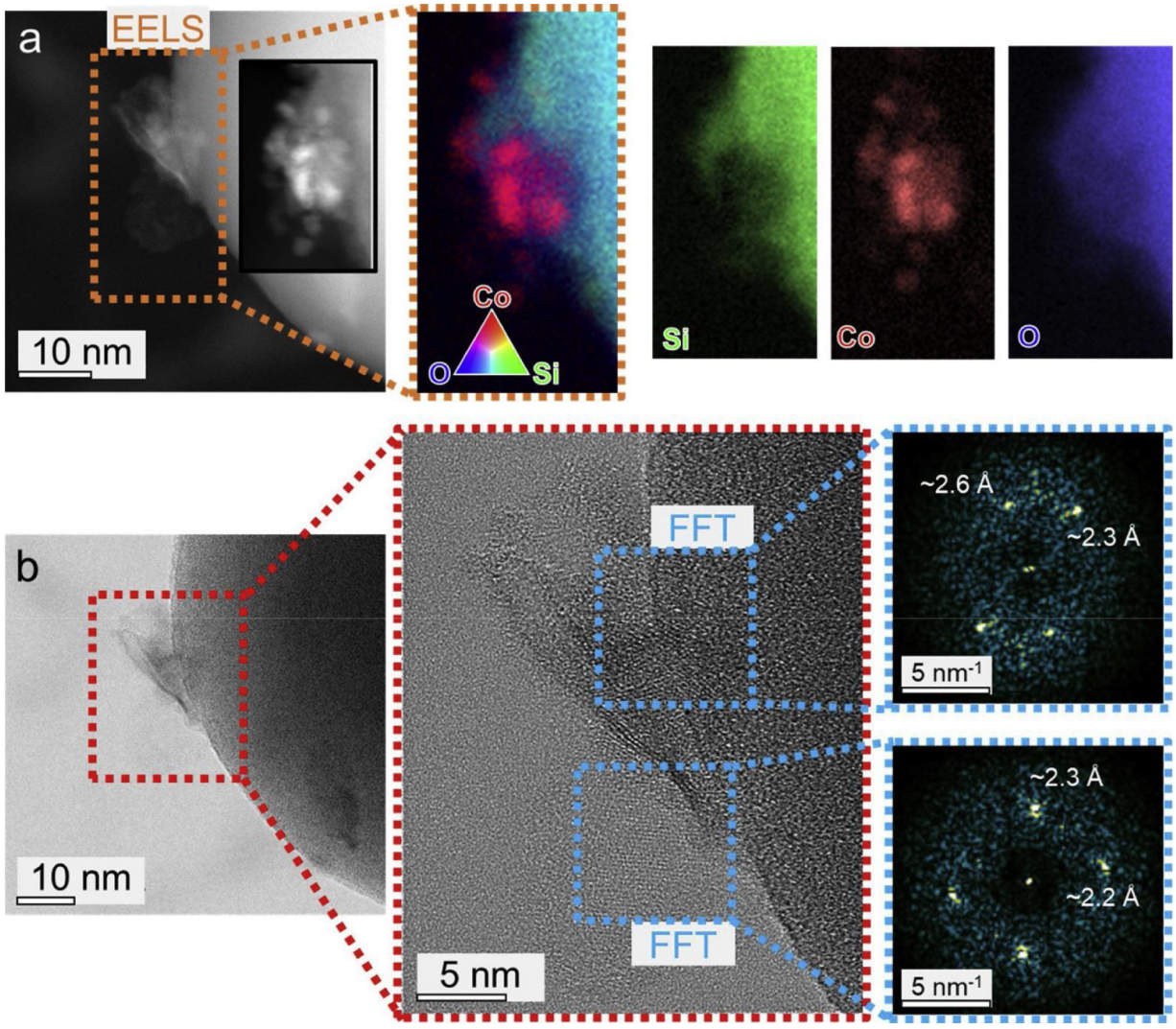

Fig. 6. (a) High-resolution high angle annular dark field micrograph with elemental mapping and separate maps for the particular elements as obtained via electron energy loss spectroscopy and (b) bright field scanning transmission electron micrograph with a magnified area and generated diffractogram patterns of a needle-type structure on a cobalt nanoparticle in the spent and passivated model catalyst CAT B1. The inset in (a) shows the analysed structure after elemental mapping exhibiting the destructive effect of the beam on the morphology with prolonged exposure time, which results in an inhomogeneous distribution of the elements.

this Co_2SiO_4 phase when compared to larger ones, which suggests that full encapsulation may be required prior to the formation of needle-type Co_2SiO_4. Both processes appear to be induced by high concentrations of H_2O, as also evidenced during the in situ magnetic characterisation of the stability of nano-sized Co crystallites on SiO_2 Stöber spheres in a previous study, which produced the spent samples for the present in-depth characterisation of MSCs.

Acknowledgments

Financial support from the DST-NRF Centre of Excellence in Catalysis (c*change), the UK Catalysis Hub, the University of Cape Town (UCT), the University College London (UCL), and the German Academic Exchange Service (DAAD) is gratefully acknowledged. Lebohang Macheli of the Catalysis Institute and c*change at UCT is gratefully acknowledged for the preparation of the Co_2SiO_4 standard.

References

[1] S.J. Tauster, Acc. Chem. Res. 20 (1987) 389–394.
[2] S.S. Tamhankar, L.K. Doraiswamy, AIChE J. 25 (1979) 561–582.
[3] P. Arnoldy, J.A. Moulijn, J. Catal. 93 (1985) 38–54.
[4] A. Kogelbauer, J.C. Weber, J.G. Goodwin Jr, Catal. Lett. 34 (1995) 259–267.
[5] D. Schanke, A.M. Hilmen, E. Bergene, K. Kinnari, E. Rytter, E. Ådanes, A. Holmen, Energy Fuels 10 (1996) 867–872.
[6] P.J. van Berge, J. van de Loosdrecht, S. Barradas, A.M. van der Kraan, Catal. Today 58 (2000) 321–334.
[7] A. Barbier, A. Tuel, I. Arcon, A. Kodre, G.A. Martin, J. Catal. 200 (2001) 106–116.
[8] G.W. Huber, C.G. Guymon, T.L. Conrad, B.C. Stephenson, C.H. Bartholomew, J.J. Spivey, G.W. Roberts, B.H. Davis (Eds.), Hydrothermal stability of Co/SiO_2 Fischer-Tropsch synthesis catalysts, vol. 139, Elsevier, Lexington, USA, 2001, pp. 423–430 Catal. Deactiv.
[9] W. Zhou, J.G. Chen, K.G. Fang, Y.H. Sun, Fuel Process. Technol. 87 (2006) 609–616.
[10] A. Tavasoli, A. Nakhaeipour, K. Sadaghiani, Fuel Process. Technol. 88 (2007) 461–469.
[11] D.J. Moodley, A.M. Saib, J. van de Loosdrecht, C.A. Welker-Nieuwoudt, B.H. Sigwebela, J.W. Niemantsverdriet, Catal. Today 171 (2011) 192–200.
[12] D. Schanke, A.M. Hilmen, E. Bergene, K. Kinnari, E. Rytter, E. Ådanes, A. Holmen, Catal. Lett. 34 (1995) 269–284.
[13] G. Jacobs, P.M. Patterson, T.K. Das, M. Luo, B.H. Davis, Appl. Catal. A Gen. 270 (2004) 65–76.
[14] R.B. Greegor, F.W. Lytle, R.L. Chin, D.M. Hercules, J. Phys. Chem. 85 (1981) 1232–1235.
[15] G. Jacobs, P.M. Patterson, Y. Zhang, T. Das, J. Li, B.H. Davis, Appl. Catal. A Gen.

233 (2002) 215–226.
[16] T.K. Das, G. Jacobs, P.M. Patterson, W.A. Conner, J. Li, B.H. Davis, Fuel 82 (2003) 805–815.
[17] G. Jacobs, T.K. Das, P.M. Patterson, J. Li, L. Sanchez, B.H. Davis, Appl. Catal. A Gen. 247 (2003) 335–343.
[18] N.E. Tsakoumis, J.C. Walmsley, M. Rønning, W. van Beek, E. Rytter, A. Holmen, J. Am. Chem. Soc. 139 (2017) 3706–3715.
[19] G. Kiss, C.E. Kliewer, G.J. DeMartin, C.C. Culross, J.E. Baumgartner, J. Catal. 217 (2003) 127–140.
[20] M.E. Dry, FT catalysts, in: A.P. Steynberg, M.E. Dry (Eds.), Fischer-Tropsch Technol. Elsevier, Amsterdam, 2004, pp. 533–600.
[21] N. Fischer, B. Clapham, T. Feltes, E. van Steen, M. Claeys, Angew. Chemie Int. Ed. 53 (2014) 1342–1345.
[22] E. Patanou, N.E. Tsakoumis, R. Myrstad, E.A. Blekkan, Appl. Catal. A Gen. 549 (2018) 280–288.
[23] M. Claeys, M.E. Dry, E. van Steen, P.J. van Berge, S. Booyens, R. Crous, P. van Helden, J. Labuschagne, D.J. Moodley, A.M. Saib, ACS Catal. 5 (2015) 841–852.
[24] M. Wolf, B.K. Mutuma, N.J. Coville, N. Fischer, M. Claeys, ACS Catal. 8 (2018) 3985–3989.
[25] E. van Steen, M. Claeys, M.E. Dry, J. van de Loosdrecht, E.L. Viljoen, J.L. Visagie, J. Phys. Chem. B 109 (2005) 3575–3577.
[26] J. van de Loosdrecht, B. Balzhinimaev, J.-A. Dalmon, J.W. Niemantsverdriet, S.V. Tsybulya, A.M. Saib, P.J. van Berge, J.L. Visagie, Catal. Today 123 (2007) 293–302.
[27] M. Sadeqzadeh, S. Chambrey, J. Hong, P. Fongarland, F. Luck, D. Curulla-Ferré, D. Schweich, J. Bousquet, A.Y. Khodakov, Ind. Eng. Chem. Res. 53 (2014) 6913–6922.
[28] P. Burattin, M. Che, C. Louis, J. Phys. Chem. B 102 (1998) 2722–2732.
[29] M. Mhamdi, E. Marceau, S. Khaddar-Zine, A. Ghorbel, M. Che, Y.B. Taarit, F. Villain, Catal. Letters 98 (2004) 135–140.
[30] J.C. Park, H.J. Lee, J.U. Bang, K.H. Park, H. Song, Chem. Commun. (Camb.) (2009) 7345–7347.
[31] J.C. Park, S.W. Kang, J.C. Kim, J.I. Kwon, S. Jang, G.B. Rhim, M. Kim, D.H. Chun, H.T. Lee, H. Jung, H. Song, J.I. Yang, Nano Res. 10 (2017) 1044–1055.
[32] A.R. Richard, M. Fan, ACS Catal. 7 (2017) 5679–5692.
[33] M. Wolf, H. Kotzé, N. Fischer, M. Claeys, Faraday Discuss. 197 (2017) 243–268.
[34] E. van Steen, G.S. Sewell, R.A. Makhothe, C. Micklethwaite, H. Manstein, M. de Lange, C.T. O'Connor, J. Catal. 162 (1996) 220–229.
[35] N. Shi, W. Cheng, H. Zhou, T. Fan, M. Niederberger, Chem. Commun. (Camb.) 51 (2015) 1338–1340.
[36] M. Wolf, N. Fischer, M. Claeys, Mater. Chem. Phys. 213 (2018) 305–312.
[37] W. Stöber, J. Colloid Interface Sci. 26 (1968) 62–69.
[38] X.-D. Wang, Z.-X. Shen, T. Sang, X.-B. Cheng, M.-F. Li, L.-Y. Chen, Z.-S. Wang, J. Colloid Interface Sci. 341 (2010) 23–29.
[39] M. Claeys, E. van Steen, J.L. Visagie, J. van de Loosdrecht, Magnetometer, US Patent 8,773,118 B2, 2014.
[40] M. Wolf, N. Fischer, M. Claeys, Catal. Today 275 (2016) 135–140.
[41] A.J. Dent, G. Cibin, S. Ramos, A.D. Smith, S.M. Scott, L. Varandas, M.R. Pearson, N.A. Krumpa, C.P. Jones, P.E. Robbins, J. Phys. Conf. Ser. 190 (2009) 012039.
[42] L.A. Bruce, J.V. Sanders, T.W. Turney, Clays Clay Miner. 34 (1986) 25–36.
[43] B. Ravel, M. Newville, J. Synchrotron Radiat. 12 (2005) 537–541.
[44] M. Newville, J. Synchrotron Radiat. 8 (2001) 322–324.
[45] A. Moen, D.G. Nicholson, B.S. Clausen, P.L. Hansen, A. Molenbroek, G. Steffensen, Chem. Mater. 9 (1997) 1241–1247.
[46] F. Farges, G. Brown, J. Rehr, Phys. Rev. B 56 (1997) 1809–1819.
[47] W. Bungmek, P. Viravathana, S. Prangsri-aroon, S. Chotiwan, O. Deutschmann, H. Schulz, Proc. Int. Conf. Environ. Ind. Innov. 12 (2011) 65–69.
[48] C. Li, X. Han, F. Cheng, Y. Hu, C. Chen, J. Chen, Nat. Commun. 6 (2015) 7345.
[49] J. Li, X. Zhan, Y. Zhang, G. Jacobs, T. Das, B.H. Davis, Appl. Catal. A Gen. 228 (2002) 203–212.
[50] A. Sirijaruphan, A. Horváth, J.G. Goodwin Jr., R. Oukaci, Catal. Lett. 91 (2003) 89–94.
[51] A. Tavasoli, K. Sadagiani, F. Khorashe, A.A. Seifkordi, A.A. Rohani, A. Nakhaeipour, Fuel Process. Technol. 89 (2008) 491–498.
[52] L.A. Zabdyr, G. Garzel, O.B. Fabrichnaya, Calphad Comput. Coupling Phase Diagrams Thermochem. 27 (2003) 127–132.
[53] A.M. Saib, A. Borgna, J. van de Loosdrecht, P.J. van Berge, J.W. Geus, J.W. Niemantsverdriet, J. Catal. 239 (2006) 326–339.
[54] N. Morimoto, M. Tokonami, M. Watanabe, K. Koto, Am. Mineral. 59 (1974) 475–485.
[55] N.E. Tsakoumis, A. Voronov, M. Rønning, W. van Beek, Ø. Borg, E. Rytter, A. Holmen, J. Catal. 291 (2012) 138–148.
[56] A. Moen, D.G. Nicholson, M. Rønning, H. Emerich, J. Mater. Chem. 8 (1998) 2533–2539.
[57] A.K. Dalai, B.H. Davis, Appl. Catal. A Gen. 348 (2008) 1–15.
[58] G.L. Bezemer, J.H. Bitter, H.P.C.E. Kuipers, H. Oosterbeek, J.E. Holewijn, X. Xu, F. Kapteijn, A.J. van Dillen, K.P. de Jong, J. Am. Chem. Soc. 128 (2006) 3956–3964.
[59] Ø. Borg, P.D.C. Dietzel, A.I. Spjelkavik, E.Z. Tveten, J.C. Walmsley, S. Diplas, S. Eri, A. Holmen, E. Rytter, J. Catal. 259 (2008) 161–164.
[60] J.P. den Breejen, P.B. Radstake, G.L. Bezemer, J.H. Bitter, A. Holmen, K.P. de Jong, J. Am. Chem. Soc. 131 (2009) 7197–7203.
[61] S. Rane, Ø. Borg, E. Rytter, A. Holmen, Appl. Catal. A Gen. 437–438 (2012) 10–17.
[62] N. Fischer, B. Clapham, T. Feltes, M. Claeys, ACS Catal. 5 (2015) 113–121.
[63] S. Lee, B. Lee, S. Seifert, R.E. Winans, S. Vajda, J. Phys. Chem. C. 119 (2015) 11210–11216.
[64] J. Yang, V. Frøseth, D. Chen, A. Holmen, Surf. Sci. 648 (2015) 67–73.
[65] W.T. Ralston, G. Melaet, T. Saephan, G.A. Somorjai, Angew. Chemie - Int. Ed. 56 (2017) 7415–7419.
[66] A. Tuxen, S. Carenco, M. Chintapalli, C.-H. Chuang, C. Escudero, E. Pach, P. Jiang, F. Borondics, B. Beberwyck, A.P. Alivisatos, G. Thornton, W.-F. Pong, J. Guo, R. Perez, F. Besenbacher, M. Salmeron, J. Am. Chem. Soc. 135 (2013) 2273–2278.
[67] P. van Helden, I.M. Ciobîcă, R.L.J. Coetzer, Catal. Today 261 (2016) 48–59.
[68] A.M. Saib, A. Borgna, J. van de Loosdrecht, P.J. van Berge, J.W. Niemantsverdriet, J. Phys. Chem. B 110 (2006) 8657–8664.
[69] A.M. Saib, A. Borgna, J. van de Loosdrecht, P.J. van Berge, J.W. Niemantsverdriet, Appl. Catal. A Gen. 312 (2006) 12–19.